Supplementary Information for: Generation of bright quantum high-order harmonic driven by combined coherent and bright squeezed vacuum light

Wentao Wang[1,2†], Yaoshun Sun[1,2†], Liyuan Wang[1,2], Lingrui Hu[3], Dajun Ding[1,2], Xiangyu Tang[1,2*], Mingxuan Li[1,2*], Jianmin Yuan[1,2*], Sizuo Luo[1,2*]

[1]Institute of Atomic and Molecular Physics, Jilin University, Changchun, 130012, China.
[2]Jilin Provincial Key Laboratory of Transient Quantum Process Control and Application, Jilin University, Changchun, 130012, China.
[3]College of Physics, Jilin University, Changchun, 130012, China.

*Corresponding author(s). E-mail(s): tangxiangyu@jlu.edu.cn; mingxuanli@jlu.edu.cn; yuanjianmin@jlu.edu.cn; luosz@jlu.edu.cn;
†These authors contributed equally to this work.

In this Supplementary Material, we provide more details about: I. Experimental setup and method, and HHG from the coherent field and quantum two-color field. II. Theoretical methods.

1 Experimental setup and method

A two-color field scheme, i.e. strong coherent 800 nm laser combined with a weak 1600 nm BSV light, is employed to generate high-order harmonics endowed with quantum properties as shown in Fig S1 (a). The laser source is a Ti:sapphire system delivering 35 fs, 7 mJ pulses at 800 nm with a 1 kHz repetition rate. The coherent laser exhibits $g^2(0) = 1.003$ as presented in Fig S1 (c). Its output is divided by a 50:50 beam splitter; one arm, with an input pulse energy of approximately 0.72 mJ, serves as the seed for generating the bright squeezed vacuum (BSV) field. The BSV is produced via type-I spontaneous parametric down-conversion (SPDC) in a 3-mm-thick β-BaB_2O_4

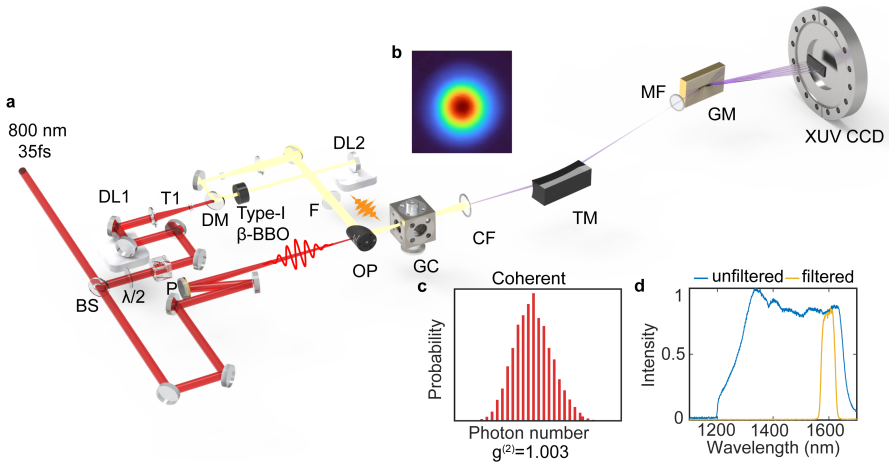

Fig. S1 (a)Illustration of the experimental methodology. BS: beam splitter; P: polarizer; DL: delay line; T: telescope; DM: dichroic mirror; F: filter; OP: off-axis parabolic mirror; GC: gas cell; CF: coaxial filter; TM: toroidal mirror; MF: metal filter; GM: grating mirror; CCD: charge-coupled device. (b) CCD image of filtered beam spot. (c) Photon-number statistics of coherent state. (d) Unfiltered (blue) and filtered (yellow) spectra.

crystal centered at 1600 nm. A double-pass configuration, using a silver mirror placed 35 cm from the crystal, selects the fundamental spatial mode and enhances phase matching for the lowest-divergence component as can be seen in Fig S1 (b). After spectral filtering using a bandpass filter (Edmund #87-872), a near-single-mode BSV is obtained with a center wavelength of 1600 nm and a bandwidth of 50 nm FWHM as shown in Fig S1 (d). The spectrum is recorded by a spectrometer (Zolix SGM1700). The filtered BSV field exhibits a second-order correlation function $g^{(2)}(0) = 2.324$, corresponding to a pulse energy of approximately 0.18 μJ.

The BSV beam is then expanded to 14 mm using a telescope. The expanded BSV beam is tightly focused by an off-axis parabolic mirror (f = 101.6 mm) with a central 3 mm hole. Meanwhile, the coherent infrared driving field (intensity $\sim 1.7\times10^{14}$ W/cm^2) is directed via a spherical mirror (f = 500 mm) through the same 3 mm hole. The mean intensity of the BSV is calculated to be $\sim 2 \times 10^{11}$ W/cm^2, corresponding to $\sim 1.5 \times 10^{12}$ photons per pulse. Spatial and temporal overlap of the two beams is verified with a CCD camera. The recombined beams are focused into a 3-mm-long gas cell containing krypton gas, where high-order harmonics are generated. To filter out the fundamental laser, the HHG radiation, and the driving laser pass through a 500-nm-thick Al foil. The produced HHG is then focused by an Au-coated toroidal mirror and sent into a home-built slit-less XUV spectrometer. Within the spectrometer, the XUV spectra are spatially dispersed by a Hitachi plane concave diffraction grating mounted on a five-axis tip-tilt alignment stage (Newport 8081M-UHV). The spectrally resolved signal is recorded with an XUV-sensitive camera (Princeton Instruments PIXIS-XO:400B).

1.1 Comparison of HHG driven by 800 nm coherent laser and 800 nm coherent laser with 1600 nm BSV

Figure S2 directly compares pressure-dependent high-order harmonic spectra driven by a strong 800 nm coherent laser ($g^2(0) = 1.003$, $\sim 1.7 \times 10^{14}$ W/cm^2) with spectra generated after adding a weak BSV light ($g^2(0) = 2.324$, $\sim 2{\times}10^{11}$ W/cm^2). The newly produced peaks arising from absorption or emission of BSV photons are discussed in detail in the main text. Here, we focus only on the influence of BSV on the main harmonic peaks (H_{2n+1}), with the pressure-dependent intensities for each harmonic are shown in Fig. S2 (c)–(h). These intensities share the same pressure dependence for the same harmonic order, demonstrating that the weak BSV only perturbatively affects the generation of the main harmonics. Consequently, the macroscopic phase matching of HHG driven by a strong 800 nm coherent laser together with a weak 1600 nm BSV light can be treated as the propagation of a coherent model with appropriate inputs based on the Husimi distribution of the BSV light.

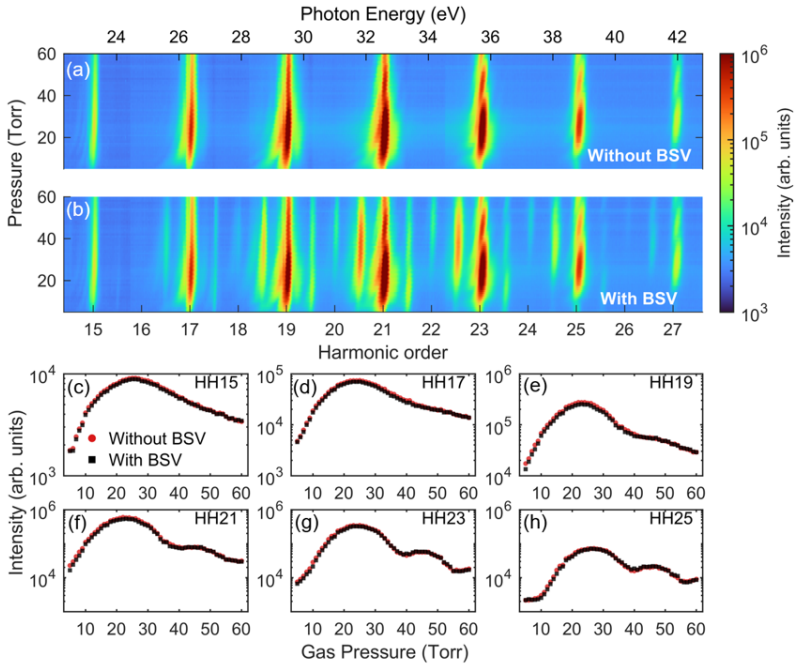

Fig. S2 (a) Harmonic yields as a function of gas pressure driven by a coherent 800 nm field ($\sim 1.7 \times 10^{14}$ W/cm^2). (b) Harmonic yields as a function of gas pressure driven by the combined 800 nm coherent field and a 1600 nm BSV field ($\sim 2 \times 10^{11}$ W/cm^2). (c)–(h) Pressure dependence of harmonic intensities for selected harmonic orders from coherent laser (red dots) and with BSV laser (black squares).

2 Theoretical method

2.1 Simulation of the two-color driving fields

The two-color laser pulse consisting of a noiseless fundamental coherent component at frequency ω ($\lambda = 800$ nm) and a stochastic component at half the frequency $\omega/2$ ($\lambda = 1600$ nm) . For each shot of driving field, its temporal electric field is formulated as

$$E(t) = \left[y_x \cos\left(\frac{\omega t}{2} + \phi\right) + y_y \sin\left(\frac{\omega t}{2} + \phi\right) + E_0 \cos(\omega t) \right] f(t). \tag{S1}$$

Here, E_0 corresponds to the amplitude of 800 nm coherent field. The parameter ϕ represents the relative phase between 1600 nm and 800 nm fields.

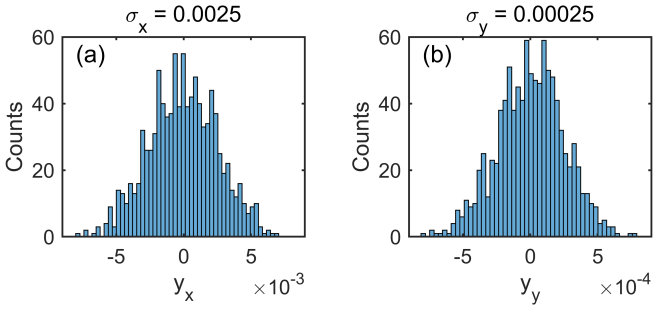

Fig. S3 Random samples of the 1600 nm amplitudes in two orthogonal quadratures.

To simulate the quantum fluctuation of the bright squeezed vacuum (BSV) state, the parameters y_x and y_y, representing the amplitudes of the two orthogonal quadratures of the stochastic $\omega/2$ component, are sampled from independent Gaussian distributions

$$G(y_i) = \frac{1}{\sqrt{2\pi}\sigma_i} \exp\left[-\frac{(y_i - \mu_i)^2}{2\sigma_i^2} \right], \tag{S2}$$

where their standard deviations, dictating the degree of squeezing and phase-space asymmetry, are $\sigma_x = 2.5\times10^{-3}$, $\sigma_y = 2.5\times10^{-4}$, and mean value $\mu_i = 0$. In simulation, 1000 samples, which have been tested to be convergent, are generated using normal random function to replicate the macroscopic squeezed vacuum statistics, as shown in Fig. S3.

The temporal pulse envelope $f(t)$ is defined as a trapezoid that incorporates a leading and trailing edge of 3 optical cycles, and a flat plateau of 8 optical cycles. The optical cycle is defined by the period of 800 nm field. In space, the laser fields of 800 nm and 1600 nm are expressed by the analytical Gaussian form

$$\widetilde{E}(r, z) = A_0 \frac{iQ(0)}{Q(z)} \exp\left(\frac{-ikr^2}{2Q(z)} \right), \tag{S3}$$

with peak amplitude A_0 and $Q(z) = z + iz_R$, where z_R is the Rayleigh length, and $k = \omega/c$ is wave numbers.

2.2 Calculation of microscopic dipole response

To obtain the microscopic dipole response of HHG, we solve the one-dimensional time-dependent Schrödinger equation (1D-TDSE) for each shot

$$i\frac{\partial}{\partial t}\Psi(x,t) = \hat{H}(t)\Psi(x,t), \tag{S4}$$

with the Hamiltonian given in atomic units ($e = m_e = \hbar = 1$) as

$$\hat{H}(t) = -\frac{1}{2}\frac{\partial^2}{\partial x^2} + V_{\text{atom}}(x) + V_{\text{abs}}(x) + xE(t). \tag{S5}$$

The krypton (Kr) atom is modeled by a short-range Pöschl-Teller potential

$$V_{\text{atom}}(x) = -\frac{V_0}{\cosh^2(\alpha x)}. \tag{S6}$$

The potential width parameter is fixed at $\alpha = 0.68$. To precisely reproduce the experimental ionization potential of krypton ($I_p = 14.00$ eV), the potential depth V_0 is dynamically optimized using the Nelder-Mead simplex algorithm, yielding an optimized value of $V_0 = 0.8596$.

Since multiple samples need calculating to simulate single-atom response by BSV field, to save computational time, we developed a GPU-accelerated deep Residual Multilayer Perceptron (ResMLP) as a surrogate model. The model bypasses the computationally expensive wavefunction propagation, directly mapping the physical driving parameters to the time-dependent dipole acceleration. This enables the rapid calculation of microscopic dipole response with high accuracy and speeds up the computation by over three orders of magnitude.

2.3 Macroscopic propagation of quantum high-order harmonics

While the ResMLP surrogate model efficiently resolves the single-atom microscopic dynamics, directly comparing theoretical predictions with experimental observables necessitates a rigorous macroscopic treatment. The macroscopic propagation of harmonic fields $\widetilde{E}_h$ is solved by Maxwell's equations in one dimension ($r = 0$) and moving frame

$$-\frac{2i\omega}{c}\frac{\partial \widetilde{E}_h(z',\omega)}{\partial z'} = \frac{2\omega^2}{c^2}\left(\delta_h + i\beta_h\right)\widetilde{E}_h(z',\omega) - \mu_0\omega^2\widetilde{P}_{\text{NL}}(z',\omega). \tag{S7}$$

Here, μ_0 is the vacuum permeability, c is the speed of light, $\tilde{n} = 1 + \delta_h + i\beta_h$ is the complex index of gas medium where δ_h and β_h account for the dispersion and absorption respectively.

The nonlinear polarization $\widetilde{P}_{NL}$ is obtained by the developed 1D-TDSE neural network, by inputting the spatiotemporal driving field $E(z',t)$. The propagation effect

of driving field incorporates the phase shift induced by Gouy phase ϕ_{geo}, dispersion from neutral ϕ_{dis} atoms and plasma ϕ_{pla}, with

$$\begin{aligned}\phi_{geo}(z') &= -\tan^{-1}(z'/z_R),\\ \phi_{dis}(z') &= \int_{z_0}^{z'} \frac{\rho\alpha_1\omega}{2\varepsilon_0 c}[1-\eta(z)]dz,\\ \phi_{pla}(z') &= -\int_{z_0}^{z'} \frac{\eta(z)e^2\rho}{2\varepsilon_0 c m_e\omega}dz.\end{aligned} \tag{S8}$$

z_R is Rayleigh length of laser beams. ρ and α_1 are density and polarizability of atoms. ω is angular frequency of laser field, and η is ionization degree of medium. ε_0 and c are permittivity and light velocity in the vacuum. e and m_e are charge and mass of electron. z_0 is the entrance position of the gas meidum. The phases are calculated for both 1600 nm and 800 nm fields, then their difference is inputted into Eq. (S1) as ϕ. For each shot of harmonic field $\widetilde{E}_h^i$, it is individually propagated through the gas medium. Finally, to obtain the expected HHG spectra $H(\omega)$, they are integrated incoherently

$$H(\omega) = \sum_i \left|\widetilde{E}_h^i(\omega)\right|^2. \tag{S9}$$

2.4 Semi-classical analysis of phase matching mechanism

The phase mismatch $\Delta k = \Delta k_{geo} + \Delta k_{dis} + \Delta k_{ele} + \Delta k_{dip}$ of harmonics during macroscopic propagation arises from four terms. Δk_{geo} is related to the Gouy phase. Δk_{dis} and Δk_{ele} are resulted from the change of refractive index of medium, connected to ionization degree, and Δk_{dip} is determined by the action phase ϕ_{act} [1]. When the 1600 nm field is weak enough, the first three are very close to those in the sole 800 nm

$$\begin{aligned}\Delta k_{geo}(z) &\approx -\frac{\omega_h}{\omega}\frac{1}{z_R}\frac{1}{1+(z/z_R)^2},\\ \Delta k_{dis}(z) &\approx \frac{\omega_h}{c}\frac{\rho(\alpha_1-\alpha_q)}{2\varepsilon_0}[1-\eta(z)],\\ \Delta k_{ele}(z) &\approx -\frac{\omega_h}{c}\frac{e^2\eta(z)\rho}{2\varepsilon_0 m_e\omega^2}.\end{aligned} \tag{S10}$$

$\hbar\omega_h$ is photon energy of harmonics, and ω and z_R are angular frequency and Rayleigh length of the 800 nm field. α_1 and α_q are polarizability of atoms at fundamental and harmonic frequency, and η is ionization degree of medium. e and m_e are charge and mass of electron, and ε_0 is permittivity in the vacuum. The Δk_{dip} and Δk_{ele} are proportional to gas pressure P by $\rho = Pk_BT$, where ρ is atoms density, k_B is Boltzmann constant and T is temperature.

The term $\Delta k_{dip} \approx \nabla\phi_{act}$, where action phase ϕ_{act} is temporal integral of Hamiltonian, can be expressed using the semi-classical strong-field approximation theory in

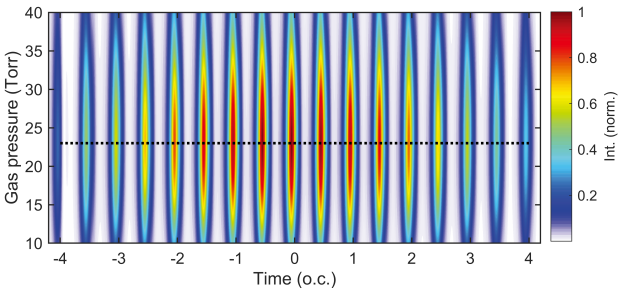

Fig. S4 Gas-pressure dependent intensity of attosecond pulses generated in coherent 800 nm field only.

atomic units ($e = 1, \hbar = 1, m_e = 1$) as

$$\phi_{act} = \int_{t_b}^{t_r} \left(\frac{[p + A(t)]^2}{2} + I_p \right) dt. \tag{S11}$$

Here, p is momentum of electron, $A(t)$ is vector potential of driving field, I_p is ionization potential of atom, and t_b and t_r are time of ionization and recombination of electron by solving classical motion of electron in the field. It can be approximated as $\phi_{act} \approx \varphi_{coh} + \sigma$, with

$$\begin{aligned} \varphi_{coh} &= \int_{t_b}^{t_r} \left(\frac{[p + A_1(t)]^2}{2} + I_p \right) dt, \\ \sigma &= \int_{t_b}^{t_r} A_2(t) \left[p + A_1(t) \right] dt, \end{aligned} \tag{S12}$$

where $A_1(t) = -A_0 \sin(\omega t)$ and $A_2(t) = -A_p \sin(\omega t/2 + \phi)$ are vector potential of 800 nm field and 1600 nm field. φ_{coh} represents the action phase accumulated in the sole 800 nm field, and σ is perturbation phase when 1600 nm field exists.

Denoting $\Delta k_{geo} + \Delta k_{ele} = aP$, where

$$a = \frac{\omega_h}{2\varepsilon_0 c k_B T} \cdot \left[(1 - \eta)(\alpha_1 - \alpha_q) - \frac{\eta e^2}{m_e \omega_1^2} \right] \tag{S13}$$

is the prefactor obtained from Eq. (S10) excluding gas pressure P, and phase-matching gas pressure $P_{opt} = P_0 + \Delta P$, the perfect phase matching is achieved when

$$(\Delta k_{geo} + aP_0 + \nabla \varphi_{dip}) + (a\Delta P + \nabla \sigma) = 0. \tag{S14}$$

In the absence of 1600 nm field, the phase-matching gas pressure is P_0, identical to the that of sole 800 nm field only, as shown in Fig. S4. When the weak 1600 nm field exists, an extra gas pressure $\Delta P = (-\nabla \sigma)/a$ is required to compensate the mismatch

resulted from σ. The σ in Eq. (S12) is further written as

$$\sigma = -A_p \int_{r_b}^{t_r} [p - A_0 \sin(\omega t)] \sin(\omega t/2 + \phi) dt, \tag{S15}$$

related to the amplitude A_p of 1600 nm field and relative phase ϕ between two fields.

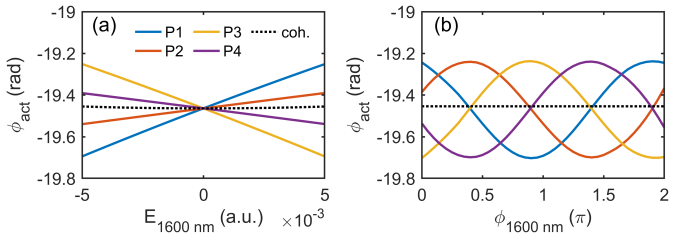

Fig. S5 Action phase with respect to four contributions (labeld by P1-P4 in Fig. 3(a) of the main text), by varying (a) amplitude of 1600 nm field, and (b) relative phase between two fields. The black dot line indicates the action phase driven by the 800 nm field only.

In Fig. S5, we calculate the ϕ_{act} corresponding to the 21st harmonic (H21) by varying the amplitude and phase of 1600 nm, where the intensity and phase of 800 nm field are fixed at 1.7×10^{14} W/cm^2 and 0 rad. The change of ϕ_{act} is well described by the trend of σ, which is proportional to the amplitude A_p of 1600 nm field, and sinusoidally oscillated with relative phase ϕ between two fields. Moreover, due to temporal symmetry of the driving field, the relation $\sigma_1 = -\sigma_3, \sigma_2 = -\sigma_4$ holds up [2], hence $\nabla\sigma_1 = -\nabla\sigma_3, \nabla\sigma_2 = -\nabla\sigma_4$.

As a result, the offset of phase-matching gas pressure satisfies $\Delta P_1 = -\Delta P_3, \Delta P_2 = \Delta P_4$, as shown in Fig. S6. Besides, the offset is opposite in sign for ϕ and $\phi + \pi$ by comparing Fig. S6 (a),(c) and (b),(d).

2.5 Phase-matching controlled pulses structure

Figure. S7 shows the normalized mean pulse intensity of after macroscopic propagation. It is clearly seen that the contrast among each contribution is tuned by gas pressure, owing to their distinguished phase-matching gas pressure.

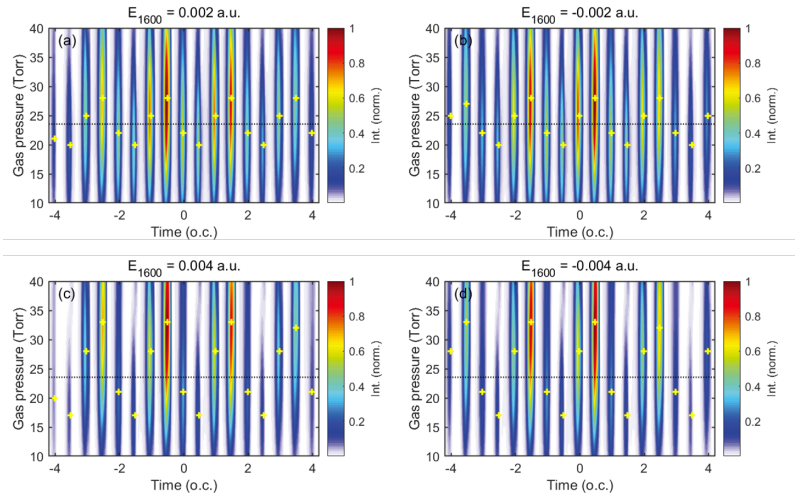

Fig. S6 Simulated attosecond pulses at different amplitudes of 1600 nm field. The relative phase between two fields is 0. Black dash lines mark the phase-matching gas pressure in 800 nm field, and yellow crosses to those in two-color field with respect to each sub burst.

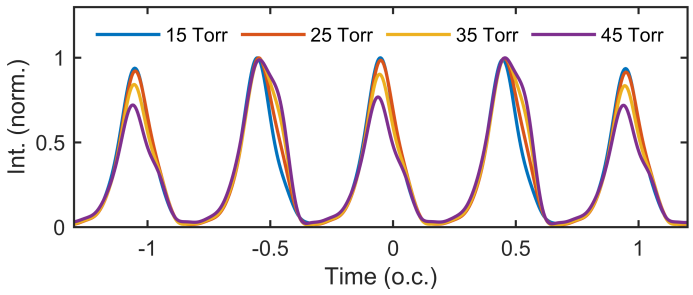

Fig. S7 Normalized mean intensity of attosecond pulses train after macroscopic propagation in simulation under four gas pressures, driven by the combined 800 nm coherent field and a 1600 nm BSV field.

References

[1] Weissenbilder, R. *et al.* How to optimize high-order harmonic generation in gases. *Nat. Rev. Phys.* **4**, 713–722 (2022).

[2] Tzur, M. E. *et al.* Attosecond-resolved quantum fluctuations of light and matter. *Preprint at https://arxiv.org/abs/2511.18362* (2025).